ACS APPLIED MATERIALS & INTERFACES

Research Article

www.acsami.org

Multifunctional Poly(L-lactide)–Polyethylene Glycol-Grafted Graphene Quantum Dots for Intracellular MicroRNA Imaging and Combined Specific-Gene-Targeting Agents Delivery for Improved Therapeutics

Haifeng Dong,*[,†] Wenhao Dai,[†] Huangxian Ju,[‡] Huiting Lu,[§] Shiyan Wang,[†] Liping Xu,[†] Shu-Feng Zhou,[⊥] Yue Zhang,*[,∥] and Xueji Zhang*[,†]

[†]Beijing Key Laboratory for Bioengineering and Sensing Technology, University of Science & Technology Beijing, Beijing 100083, P.R. China

[‡]State Key Laboratory of Analytical Chemistry for Life Science, Department of Chemistry and Chemical Engineering, Nanjing University, Nanjing 210093, P.R. China

[§]Department of Environmental Science and Engineering, School of Chemistry and Environment, Beijing University of Aeronautics & Astronautics, Beijing 100083, P.R. China

[⊥]Department of Pharmaceutical Sciences, College of Pharmacy, University of South Florida, Tampa, Florida 33612, United States

[∥]School of Materials Science and Engineering, University of Science & Technology Beijing, Beijing 100083, P.R. China

Supporting Information

ABSTRACT: Photoluminescent (PL) graphene quantum dots (GQDs) with large surface area and superior mechanical flexibility exhibit fascinating optical and electronic properties and possess great promising applications in biomedical engineering. Here, a multifunctional nanocomposite of poly(L-lactide) (PLA) and polyethylene glycol (PEG)-grafted GQDs (f-GQDs) was proposed for simultaneous intracellular microRNAs (miRNAs) imaging analysis and combined gene delivery for enhanced therapeutic efficiency. The functionalization of GQDs with PEG and PLA imparts the nanocomposite with super physiological stability and stable photoluminescence over a broad pH range, which is vital for cell imaging. Cell experiments demonstrate the f-GQDs excellent biocompatibility, lower cytotoxicity, and protective properties. Using the HeLa cell as a model, we found the f-GQDs effectively delivered a miRNA probe for intracellular miRNA imaging analysis and regulation. Notably, the large surface of GQDs was capable of simultaneous adsorption of agents targeting miRNA-21 and survivin, respectively. The combined conjugation of miRNA-21-targeting and survivin-targeting agents induced better inhibition of cancer cell growth and more apoptosis of cancer cells, compared with conjugation of agents targeting miRNA-21 or survivin alone. These findings highlight the promise of the highly versatile multifunctional nanocomposite in biomedical application of intracellular molecules analysis and clinical gene therapeutics.

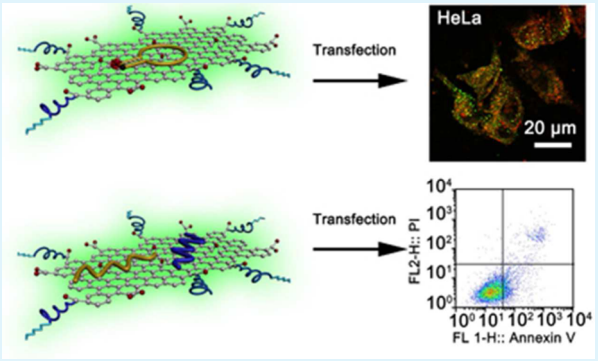

KEYWORDS: *graphene quantum dots, microRNAs, survivin, cell imaging, gene therapeutics*

INTRODUCTION

Gene therapy is mainly the introduction of a tumor-suppressor gene into the target area to inhibit tumor growth and has attracted considerable attention from researchers for its potential application in cancer treatment.[1,2] A major challenge in terms of clinical applications of gene therapy is the safe and efficient delivery of genes into cancer cells.[3,4] Various viruses,[5] polymeric particles,[6] liposomes,[7] and nanomaterials[8] have been developed for powerful gene vector systems. Among these carriers, nanomaterials with the match size of biological molecules and unique properties demonstrate advantages in gene delivery because of the large surface area/loading capacity and versatile chemistry.[9] In particular, multifunctional nanomaterials combined two or more functions including agent delivery, imaging, and therapy. These functions have the potential to improve the therapeutic efficacy.

As a particularly versatile type of graphene,[10] nanosized zero dimension photoluminescent (PL) graphene quantum dots (GQDs) possess enormous novel chemical and physical properties due to the quantum confinement and edge effects,[11]

Received: March 31, 2015
Accepted: May 5, 2015
Published: May 5, 2015

DOI: 10.1021/acsami.5b02803
ACS Appl. Mater. Interfaces 2015, 7, 11015–11023

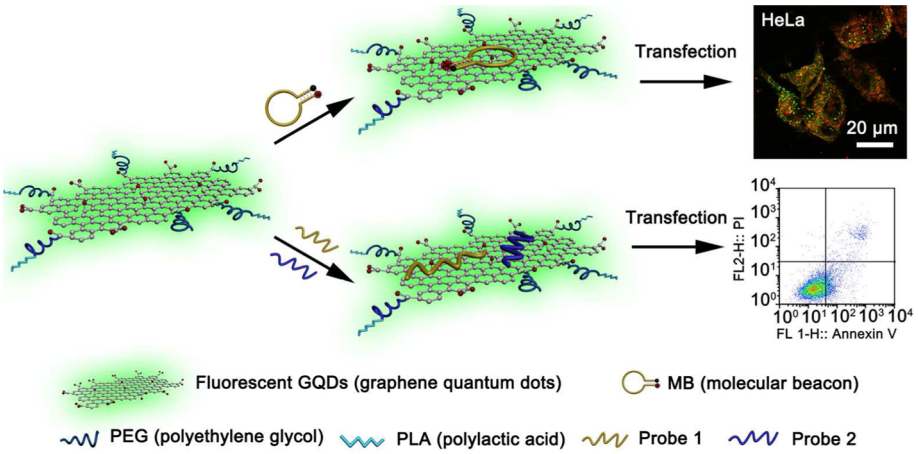

Figure 1. Schematic presentation of f-GQDs-based cell imaging and combined specific gene-targeting agents delivery. Probe 1 is the inhibitor probe of miRNA-21, and probe 2 is survivin antisense oligodeoxynucleotide.

which have generated great excitement for photovoltaic devices and biological application.[12,13] Especially in a biological system, GQDs have emerged as an alternative to replace semiconductor quantum dots for the bioimaging and fluorescent labels due to their low toxicity and eco-friendly nature.[14,15] The large surface available for efficient molecular loading and functionalization has been continuously explored as a novel nanocarrier for drug and gene delivery.[16,17]A promising system for fluorescence imaging and targeted drug delivery based on multifunctional GQDs conjugated layered protonated titanate nanoflowers has been developed.[18] A ligand-modified GQDs system for selective cell labeling, targeted drug delivery, and real-time monitoring of cellular uptake without the need for external dyes has been reported.[19] Hyaluronic acid functionalized green fluorescent GQDs-labeled human serum albumin nanoparticles with improved safety have been developed for effective drug delivery and cancer chemotherapy.[20] In order to improve the biological performance of GQDs, intensive research is ongoing to rationalize functionalization of GQDs to render them with aqueous physiological stability, good biocompatibility, and enhanced fluorescence properties.[21,22]

Recently, microRNAs (miRNAs) have emerged as one of the most promising candidates for targeting specific genes in gene therapy. MiRNAs are single-stranded, short (approximately 19−23 nucleotides), endogenous, noncoding RNAs that play a key role in various biological[23−26] and pathological processes.[27,28] The dysregulated expression of miRNAs is associated with various tumors. Thus, miRNAs have emerged as useful diagnostic markers and therapeutic targets for tumor cells.[29−31] Survivin is a new member of the inhibitor of apoptosis protein family, which can promote cellular mitosis and inhibit cellular apoptosis associated with cancer by inhibiting apoptosis protein caspase-3 and caspase-7.[32,33] These properties are quite useful in cancer diagnosis and gene therapy.[34] One emerging way of improved therapeutic efficacy has been achieved through combining therapies with different mechanisms.[35−38] A multifunctional nanocomposite of gold nanoshells on silica nanorattles has been developed for a combination of photothermal therapy and chemotherapy with low systemic toxicity.[37] The synergistic effect of chemo-photothermal therapy was observed in a doxorubicin-loaded polyethylene glycol (PEG)-ylated nanographene oxide system.[38] Co-delivery two kinds of siRNA against two different mechanisms had been reported, which displayed a synergistic effect on overcoming multidrug resistance.[39] MiRNA-499 and miRNA-133 have been proposed to act in a synergic manner to induce P19 differentiation into cardiomyocytes.[40] However, to the best of our knowledge, the combination of agents targeting miRNAs and survivin gene to investigate the enhanced cancer therapeutic efficiency by an efficient and safe delivery system still remains unexplored.

In this work, we have developed a facile and multifunctional fluorescent nanocomposite for cell imaging, intracellular miRNAs regulation, and multiple gene probe delivery to enhance gene therapeutic efficacy. As shown in Figure 1, a positive charged polymer of biocompatible PEG and biodegradable polyactic acid (PLA) was covalently grafted on the GQDs to develop a safe and efficient multifunctional GQDs (f-GQDs) nanocarrier. Specific-gene probes were loaded on the surface of the f-GQDs by specific adsorption and $\pi-\pi$ interaction between the probes and GQDs. The uptake of a multifunctional GQDs probe by HeLa cells can be monitored by the GQDs intrinsic PL, while the fluorescence of the gene probe produced by recognizing the target is employed to monitor the regulation to the target gene. We report the design, synthesis, and evaluation of the f-GQDs in intracellular miRNAs imaging analysis and regulation. The capacity of f-GQDs in the efficient loading of multiple gene probes targeting miRNA-21 and the survivin gene for enhanced gene therapeutic efficacy was investigated. We suggest that the f-GQDs nanocomposite has great potential application in intracellular molecule analysis and clinical gene therapeutics.

EXPERIMENTAL SECTION

Synthesis of the GQDs. According to the typical procedure, the GQDs were synthesized as previously reported with brief modification.[41] Briefly, the graphite power was sonicated to obtain graphene. The resulting 50 mg graphene was then added into a 50 mL nitration mixture solution (98% concentrated H_2SO_4 and 65% concentrated HNO_3 with a volume ratio of 1:3) to oxidize for 10 h at 90 °C circulation reflux. An amount of 250 mL purified water was then added into the mixture and was left overnight. The supernatant liquor was removed, and the precipitate was centrifuged and washed with water several times to remove the acids. Then, the resulting GO was dispersed in 40 mL of purified water and turned the pH to 8.0. The suspension was then transferred to a poly(tetrafluoroethylene) (Teflon)-lined autoclave (50 mL) and heated at 200 °C for 10 h to prepare the graphene quantum dots. The resulting mixture was then dialyzed several days to obtain purified GQDs.

DOI: 10.1021/acsami.5b02803
ACS Appl. Mater. Interfaces 2015, 7, 11015−11023

Synthesis of the GQDs−PEG−PLA Conjugate. In order to conjugate the PEG to GQDs via 1-ethyl-3-(3-(dimethylamino)propyl) carbodiimide (EDC) and *N*-hydroxy-succinimide (NHS) coupling, the solution of GQDs (280 μg/mL) with EDC (40 mg, 10.5 mM) and NHS (8.6 mg, 3.5 mM) was reacted for 15 min, respectively, to activate the carboxyl group. NH_2−PEG−NH_2 (M_w = 2 kDa, 1.25 mM) was then added to the activated carboxyl GQDs solution, and the solution was kept in the dark overnight. The resulting solution was dialyzed in a 3500 Da dialysis membrane for 4 days to remove the unreacted PEG. Then, PLA with an activated carboxyl group (PLA-COOH) (0.35 mM) was covalently linked to PEG conjugated GQDs (GQDs-PEG) by an EDC/NHS reaction with a similar procedure and dialyzed against an 8000−12 000 Da dialysis membrane to obtain the purified f-GQDs.

Protective Properties of f-GQDs. An amount of 5 μL of the obtained f-GQDs (1 mg/mL) was mixed with 0.5 μL of survivin antisense oligodeoxynucleotide (ASODN) (100 mM) and sonicated for 30 min to prepare f-GQDs/ASODN conjugates, and then the conjugates were treated with DNase I (1 unit) for 5 or 15 min. Samples were then analyzed with a gel electrophoresis experiment. As a comparison, the ASODN was treated with DNase I with the same procedure.

Cell Culture. The HeLa cells were cultured in Dulbecco's modified Eagle's medium (DMEM, GIBCO) supplemented with 10% fetal calf serum, penicillin (100 mg/mL), and streptomycin (100 mg/mL) at 37 °C in a humidified atmosphere containing 5% CO_2.

Cytotoxicity of f-GQDs. HeLa cells (5.0×10^4) were cultured for 12 h in a 96-well plate containing DMEM (100 μL) in each well, and then the medium was replaced with fresh serum-free medium (Opti-MEM) alone or medium containing f-GQDs and incubated for another 4 h. Next, (3-(4,5-dimethyl-2-thiazolyl)-2,5-diphenyl-2-*H*-tetrazolium bromide) MTT (20 μL, 5 mg/mL) with fresh DMEM (100 μL) was then added to each well. The media was removed 4 h later, and sodium dodecyl sulfate (100 μL) was added to solubilize the formazan dye. After shocking (37 °C, 120 rpm) for 15 min, the absorbance of each well was measured using a Tecan Sunrise at 488 nm. As a comparison, the cytotoxicity of GQDs and PEG-GQDs was investigated with the same procedure. The cytotoxicity of f-GQDs was estimated by the percentage of growth inhibition calculated with the formula.

$$\text{Growth inhibition } \% = (1 - A_{\text{text}}/A_{\text{control}}) \times 100\%$$

Intracellular miRNAs Regulation and Analysis. HeLa cells (1.0×10^4) were cultivated on glass cover slides loaded in 24-well culture plates containing DMEM (500 μL) for 12 h. The medium was then replaced with fresh Opti-MEM (500 μL) alone as a control or fresh Opti-MEM containing f-GQDs (14 μg/mL, 50 nM loaded IP) and cultivated for 4 h. After washing each well twice by phosphate-buffered saline (PBS) (0.1 M, pH = 7.4), the fresh DMEM medium (500 μL) was added and cultured for 48 h. In order to detect the concentration of miRNA-21, Opti-MEM (500 μL) containing f-GQDs (14 μg/mL, 50 nM loaded MB) was added in the cells with or without inhibitor probe (IP) treatment. The medium was removed 4 h later and incubated in DMEM for another 12 h for detection by a laser scanning microscope (CLS, 710 META, Zeiss, Germany).

Apoptosis Experiments. The cells (1×10^5) per well were seeded for 12 h in a six-well plate containing DMEM (2 mL) in each well. The medium was then replaced with fresh Opti-MEM (2 mL) or Opti-MEM (2 mL) containing f-GQDs (14 μg/mL), f-GQDs/inhibitor probe (IP) (14 μg/mL, 50 nM loaded IP), f-GQDs/ASODN (14 μg/mL, 50 nM loaded ASODN), or f-GQDs/IP/ASODN (14 μg/mL, 50 nM loaded ASODN and IP) and incubated at 37 °C for 4 h. The medium was then replaced with DMEM and cultivated for another 12 h. Afterward, the cells were trypsinized, harvested, rinsed with PBS, resuspended, and stained with Annexin V-FITC/PI according to the manufacturer's instruction. Finally, the HeLa cells were analyzed by flow cytometry (FACS, BD, USA). All experiments were detected with at least 10 000 cells, and the data were analyzed with FlowJo.

RESULTS AND DISCUSSION

Characterization of f-GQDs. Atomic force microscopy (AFM) and transmission electron microscope (TEM) images give the morphological information on graphene oxide (GO), GQDs, and f-GQDs. The size of GO made from a nitration mixture treatment mainly ranges from 200 to 300 nm by TEM analysis (Figure 2A), which was supported by the AFM

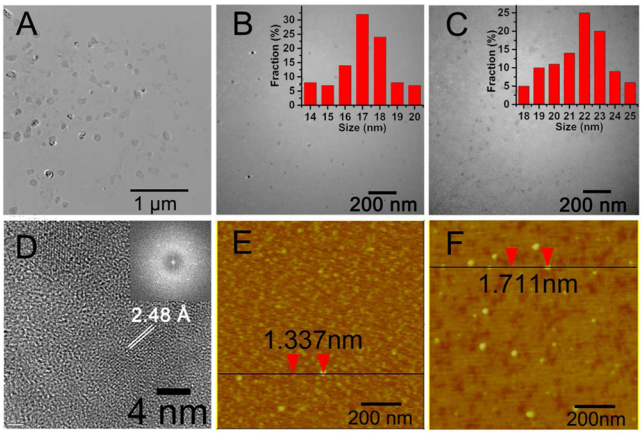

Figure 2. TEM and AFM characterization images of as-prepared GO, GQDs, and f-GQDs. TEM image of (A) GO, (B) GQDs, and (C) f-GQDs; (D) HRTEM of GQDs; AFM image of (E) GQDs and (F) f-GQDs. Inset B and C: the size distribution of the as-prepared GQDs and f-GQDs. Inset D: FFT pattern of GQDs.

observation (Figure S1, Supporting Information). The TEM image of GQDs shows the hydrothermal route cuts the preoxidized GO into unified GQDs with a diameter of about 17 nm (Figure 2B). As shown in Figure 2E, the cross-sectional view of the AFM image of the resulting GQDs shows a single layer with an average thickness of about 1.337 nm, concurring with some previous reports attributing ∼1.0 nm to a single layer.[41,42] As expected, the high-resolution TEM (HRTEM) image in Figure 2D shows the lattice constant of GQDs is 2.48 Å, in agreement with a previous report.[43] The fast Fourier transformation (FFT) presents the 6-fold symmetry feature of graphene with a hexagonal pattern (Figure 2D).[43] The functional procedure induced the size increase, as shown in Figure 2C. The lateral size of f-GQDs was mainly about 22 nm, appearing with a 5 nm increase compared to the GQDs (Figure 2B) and PEG-grafted GQDs (PEG-GQDs) (Figure S2, Supporting Information). Meanwhile, the functionalization of GQDs with PEG and PLA led to a height increase from 1.337 nm (Figure 2E) to 1.711 nm (Figure 2F), which resulted from the polymer grafted on the surface of the GQDs.

The X-ray-photoelectron spectroscopy (XPS) characterization depicts the change of the C 1s group during the hydrothermal route. The intensities of C 1s XPS peaks of epoxy, alkoxy, and carbonyl groups decreased dramatically, while the intensity of the peak assigned to the COOH group increased (Figure 3A,B). The reason might be that more C−C and C═C bonds in GO were broken, resulting in more periphery carbons which were simultaneously oxidized into the COOH group when GO changes to GQDs.[44] The Fourier transform infrared (FT-IR) spectra and electrochemical impedance spectra (EIS) analysis were used to characterize the formation of the f-GQDs. The spectrum of f-GQDs (Figure 3C, curve a) presented the characteristic peaks of PLA (curve

DOI: 10.1021/acsami.5b02803
ACS Appl. Mater. Interfaces 2015, 7, 11015−11023

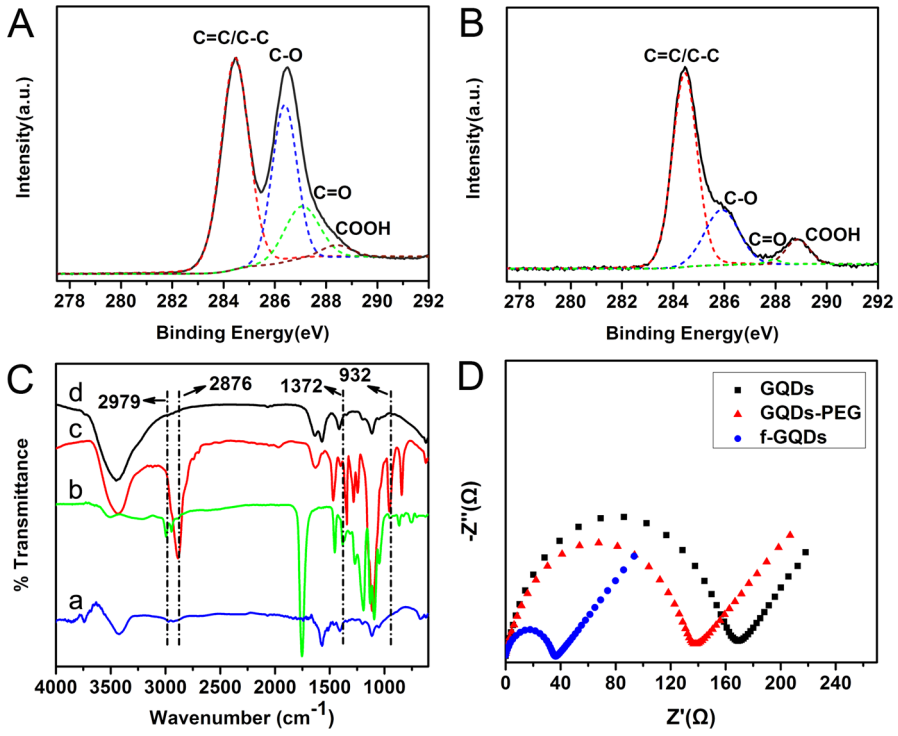

Figure 3. Compositional characterization of GO, GQDs, and f-GQDs. High-resolution XPS C 1s spectra of (A) GO and (B) GQDs; FT-IR spectra (C) of f-GQDs (a), PLA (b), PEG (c), and GQDs (d); EIS (D) of GQDs, PEG-GQDs, and a f-GQDs modified glass carbon electrode in 0.1 M KCl containing 5 mM $K_3[Fe(CN)_6]/K_4[Fe(CN)_6]$.

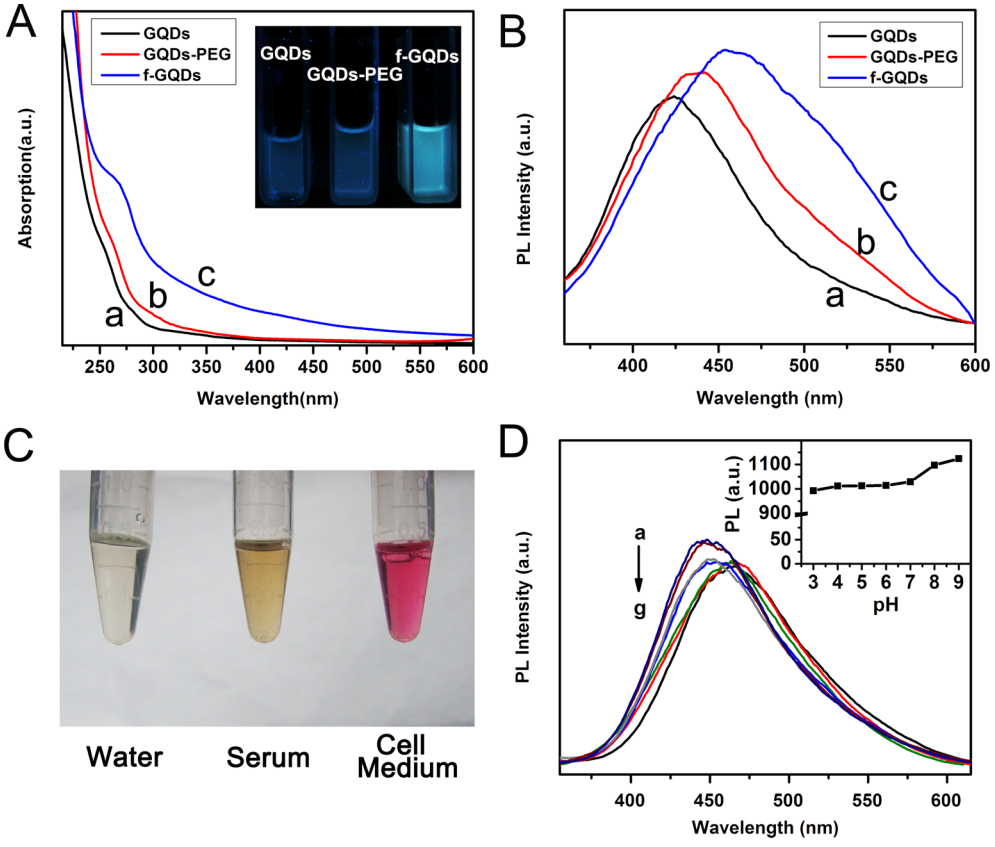

Figure 4. PL and stability properties of f-GQDs. (A) UV−vis absorption and (B) PL spectra (at 320 nm excitation) of as-prepared GQDs (a), PEG-GQDs (b), and f-GQDs (c) in water. Inset (A) is a photograph of GQDs, GQDs-PEG, and a f-GQDs aqueous solution under UV irradiation (365 nm). (C) Photograph of the f-GQDs in different mediums taken under visible light. (D) pH-dependent PL spectra when pH is switched between 9 and 3. Inset D: plot of PL intensity over pH 3−9.

DOI: 10.1021/acsami.5b02803
ACS Appl. Mater. Interfaces 2015, 7, 11015−11023

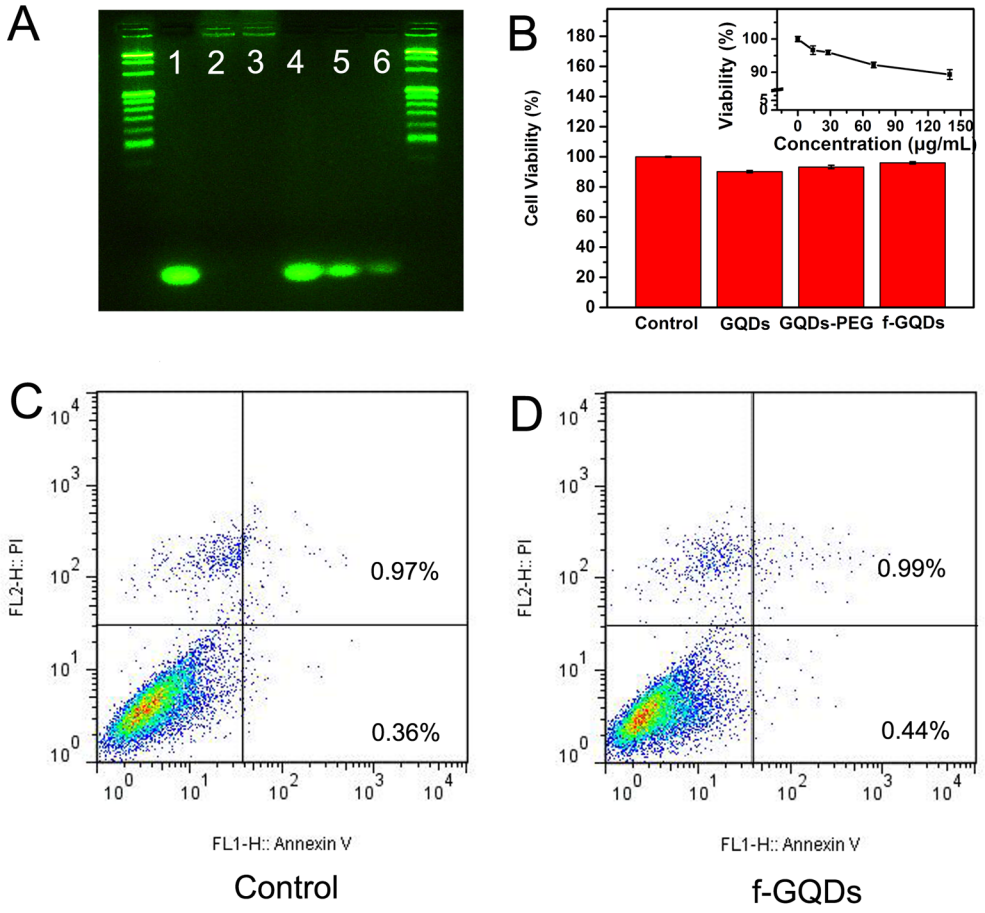

Figure 5. Protective properties and cytotoxicity of f-GQDs. (A) Image of gel electrophoresis of ASODN and f-GQDs/ASODN with and without DNase I treatment. Lane 1: ASODN only; lanes 2 and 3: ASODN treated with DNase I for 5 and 15 min, respectively; lane 4: f-GQDs/ASODN; lanes 5 and 6: f-GQDs/ASODN treated with DNase I for 5 and 15 min, respectively. (B) Cytotoxicity induced by GQDs (14 μg/mL), PEG-GQDs (14 μg/mL), and f-GQDs (14 μg/mL) of HeLa cells. Inset: Cytotoxicity induced by f-GQDs at different concentrations (14, 28, 70, 140 μg/mL). Flow cytometric analysis of apoptosis of (C) HeLa cells and (D) f-GQDs transfected-HeLa cells.

b), PEG (curve c), and GQDs (curve d), indicating the successful conjugation of PEG and PLA on the GQDs. The bending peak at 2979 cm^{-1} and stretching vibration peak at 1372 cm^{-1} of $-CH_3$ (curve b) in PLA were observed in f-GQDs (curve a). A $-CH_2-$ stretching vibration loaded at 2876 cm^{-1} and a stretching vibration $-C-O-C-$ at 932 cm^{-1} from PEG (curve c) were found in f-GQDs (curve a). The strong and broad absorption peak loaded at 3400 cm^{-1} was attributed to the $-OH$ groups in PEG (curve b) and GQDs (curve d), and the carboxyl group peak of PLA (curve b) and GQDs (curve d) at 1048 cm^{-1} were also presented in f-GQDs. The obvious absorption peaks corresponded to the amide bands I (1635 cm^{-1}) and II (1574 cm^{-1}) (curve a) of $-CONH-$ groups in the PEG and PLA functionalized GQDs.[45] Figure 3D provides a comparison between the EIS recorded at GQDs, PEG-GQDs, and f-GQDs modified glassy carbon electrodes. Compared to GQDs with an electron-transfer resistance of 170 Ω, the PEG-GQDs showed a smaller electron-transfer resistance of about 140 Ω, while f-GQDs displayed a sharp decrease in the electron-transfer resistance down to 36 Ω. This resistance was due to the positive charge of PEG and PLA, which facilitated the electron transfer of negatively charged $Fe(CN)^{3-/4-}$, suggesting that the PEG and PLA were successfully conjugated on GQDs.[46] Similarly, it was observed that the positive-charged polymer conjugation procedure induced the zeta potential decrease (Figure S3, Supporting Information), which further confirmed the successful assembly of f-GQDs.

Optical Properties and Stability of f-GQDs. By using different surface passivation agents, one can significantly modify the PL properties of GQDs and imparted GQDs with good solubility.[47] The maximum absorption peak of GQDs was located at 255 nm (Figure 4A, curve a), which appeared to red shift to 263 and 270 nm in PEG-GQDs (curve b) and f-GQDs (curve c), respectively, due to the presence of PEG and PLA. The solution color changed from light blue to deep blue due to the significantly increased absorbance (Figure 4A, inset). The as-prepared GQDs showed a strong PL peak at 425 nm when excited at 320 nm (Figure 4B, curve a). The maximum emission peak of PEG-GQDs (curve b) and f-GQDs (curve c) red-shifted to 436 and 456 nm with the 1.1- and 1.21-fold increase of intensity, respectively. The excitation-dependent PL behavior of GQDs was also observed after the functionalization (Figure S4, Supporting Information). These results suggested that the surface passivation by PEG and PLA imparted a strong influence on the optical properties of GQDs due to a change in chemical functional groups.[48] As shown in Figure 4C, the f-GQDs exhibited excellent stability in aqueous solution and protein solution: including cell medium or serum. This resulted from the hydrophilic PEG and PLA chain extending into the aqueous phase while solubilizing and stabilizing the f-GQDs in physiological conditions. The PL intensity exhibited good

DOI: 10.1021/acsami.5b02803
ACS Appl. Mater. Interfaces 2015, 7, 11015−11023

stability in acid solution and neutral solution (pH 3.0−7.0), with only a slight decrease compared to the intensity in alkaline solution (pH 9.0) (Figure 4D). The fluorescence quantum yield of f-GQDs measured by using quinine sulfate as a reference is 6.2%, similar to hydrothermal GQDs reported previously.[41] Furthermore, the time-resolved fluorescence spectrum measured with an excitation at 320 nm showed that the fluorescence lifetime of as-prepared f-GQDs is 4.00 ns (Figure S5, Supporting Information). The superior fluorescence stability of f-GQDs over a broad pH range is vital for biomedicial application.[42]

Protective Property and Cytotoxicity of f-GQDs. An effective delivery system should protect the cargos from nuclease digestion during prolonged transport.

For the f-GQDs, the gene probe can be protected from digestion by DNase I nuclease enzyme cleaving an oligodeoxynucleotide (Figure 5A). It was observed that the free gene probe was almost digested when incubated with DNase I for 5 min (lane 2) and completely hydrolyzed after 15 min incubation (lane 3). However, no obvious digestion was observed for the gene probe loaded on f-GQDs both at 5 min (lane 5) and 15 min (lane 6) incubation. The protective property possibly resulted from the steric hindrance effect preventing DNase I from accessing the gene probe. 3-(4,5-Dimethyl-2-thiazolyl)-2,5-diphenyl-2-*H*-tetrazolium bromide (MTT) assay and apoptotic experiments were carried out to investigate the cytotoxicity of f-GQDs. As shown in Figure 5B, after the HeLa cells were cultivated in media containing GQDs, PEG-GQDs, or f-GQDs for 4 h, the f-GQDs-tranfected cells showed 96% higher cell viability. This result was higher than the GQDs-tranfected cells with 90% cell viability and PEG-GQDs-transfected cells with 93% cell viability, respectively. These findings suggested the functionalization of the negative polymer of PEG and PLA rendered the f-GQDs good biocompatibility, which is similar to those observed in PEGylated graphene nanoribbons reported previously.[49] By incubating HeLa cells with f-GQDs in various concentrations, just a slight reduction of cell viability was observed for extremely high concentrations (140 μg/mL) (Figure 5B, inset). These results suggested that the f-GQDs were of low cytotoxicity and were a promising gene vector. Apoptosis analysis further confirmed the low cytotoxicity of f-GQDs; the f-GQDs-transfected cells (Figure 5D) displayed a negligible increase in apoptotic ratio compared to the control group (Figure 5C).

Intracellular MiRNA Imaging Analysis and Regulation. Considering their good optical property, excellent biocompatibility, and superior physiological stability, the fluorescent f-GQDs were employed for living cell imaging and gene probe delivery for intracellular miRNAs analysis. It was reported that GO could bind and quench a dye-labeled single-stranded DNA (ssDNA) probe, upon hybridization with the target to form a duplex structure. The fluorescence that was recovered resulted from the dissociation of the duplex from GO.[17] In this system, we designed a molecular beacon (MB) detection probe targeting miRNA-21 conjugated to the f-GQDs (f-GQDs/MB) through a $\pi-\pi$ interaction to assess the capability of the f-GQDs as a gene vector. As shown in Figure 6, observation of the green fluorescence from the f-GQDs inside the cell indicated f-GQDs were efficiently transfected into the cell (Figure 6B, green field). This agrees with a previous report that the GO can be internalized through a clathrin-mediated endocytosis process into the cytoplasm.[50] Upon the hybridization of the MB detection probe with intracellular target miRNAs-21, the fluorescence dye separated from the quencher, and the dissociation of the duplex structure from the surface of f-GQDs produced red fluorescence (Figure 6C, red field). As shown in Figure 6D, the overlay of the bright field (Figure 6A), green field (Figure 6B), and red field (Figure 6B) indicated the nanocomposite was mainly located in the cytoplasm, and the MB probe was effectively released from the f-GQDs in order to recognize the target miRNA.

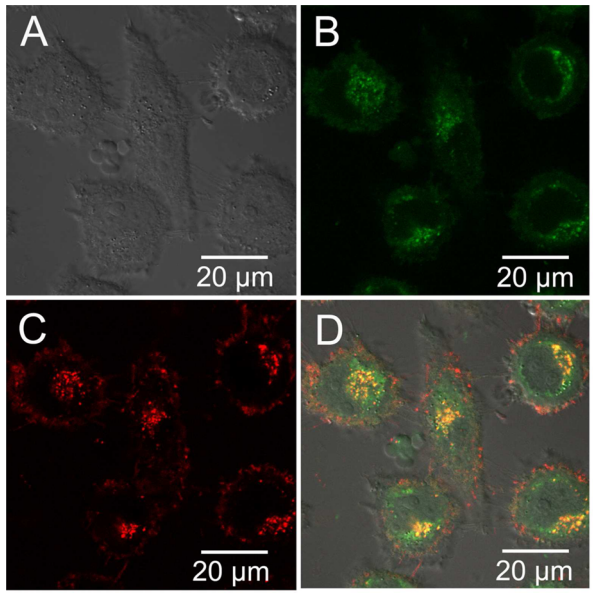

Figure 6. Confocal microscopic images of HeLa cells transfected by f-GQDs/MB (14 μg/mL, 50 nM linked MB). (A) Bright field; (B) green field; (C) red field; (D) overlapped image.

MiRNAs disregulation is associated with various human cancers. Thus, methods to regulate intracellular miRNAs are useful in clinical diagnosis and gene therapy. The inhibitor probe of miRNA-21 was loaded on f-GQDs (f-GQDs/IP) to down-regulate the level of the miRNA-21. The intracellular miRNA-21 level was analyzed by the red fluorescence intensity after delivery of f-GQDs/MB into the cells.

After the cells were incubated with the f-GQDs/IP for 48 h to inhibit the miRNA expression following transfection by f-GQDs/MB, the fluorescence intensity from MB (Figure 7E, red field) was 67.3% of that without miRNA-21 down regulation (Figure 7B, red field). The stronger green fluorescence intensity of Figure 7D compared to Figure 7A resulted from the increased accumulation of f-GQDs in the cell after two transfections. These results suggested that the intracellular miRNA levels were effectively inhibited, and the designed multifunctional GQDs were useful for both imaging and regulation of intracellular miRNAs.

Enhanced Gene Therapeutic Efficacy via Multiple Gene Probe Delivery. The large specific surface of f-GQDs was beneficial to the combined agents (IP and ASODN) (f-GQDs/IP/ASODN), targeting miRNA-21 and the survivin gene, for enhancing the gene therapeutic efficacy. As shown in Figure 8A, the cells transfected with f-GQDs/IP/ASODN exhibited a cell viability of 68%, lower than cells transfected with f-GQDs loaded with either IP (f-GQDs/IP) with a cell viability of 82% or ASODN (f-GQDs/ASODN) with a cell viability of 76%. This demonstrated that the combination of specific gene-targeting agents was useful for induction of better

DOI: 10.1021/acsami.5b02803
ACS Appl. Mater. Interfaces 2015, 7, 11015−11023

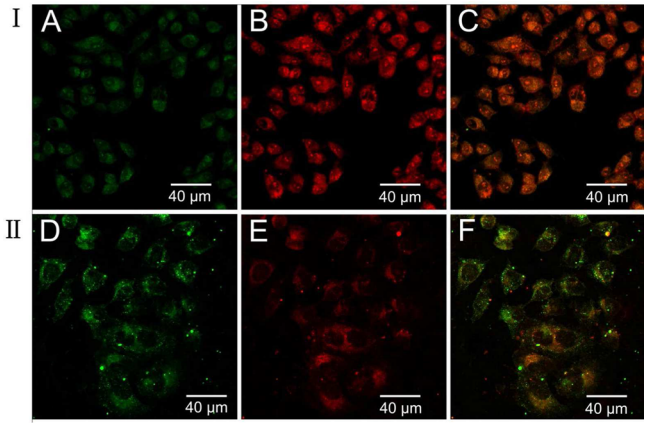

Figure 7. Confocal microscopic images of f-GQDs/MB-HeLa cells with or without IP treatment. (I) Confocal images of HeLa cells transfected with f-GQDs/MB (14 μg/mL, 50 nM linked MB) at 37 °C for 4 h. (II) HeLa cells first transfected by f-GQDs/IP (14 μg/mL, 50 nM linked IP) at 37 °C for 4 h and detected with f-GQDs/MB (14 μg/mL, 50 nM linked MB) 48 h later. (A,D) Green field; (B,E) red field; (C,F) overlapped images.

inhibition of cancer cell growth. The combined effect was further confirmed by apoptotic analysis, which was evaluated by Annexin-V-FITC and PI staining. The f-GQDs/ASODN transfected cells showed an apoptotic ratio of 7.25% (Figure 8B), 20-fold higher than the control group (Figure 5C). The f-GQDs/IP transfected cells displayed a 37-fold higher apoptotic ratio than the control group, while the f-GQDs/IP/ASODN-transfected cells presented a 43.8-fold apoptotic ratio of the control group, higher than cells transfected with f-GQDs loaded with ASODN or IP alone. The improved inhibition of cancer cell growth and additional apoptosis of the cancer cell might be explained by the possibility that both miRNA-21 and survivin could inhibit the activity of caspase-3 and caspase-7.[51,52] The phosphatase and tensin homologue deleted on chromosome ten are putative targets of miRNA-21, while survivin is an inhibitor of caspase-3 and caspase-7, which is the most important antiapoptotic protein associated with microtubules and the mitotic spindle, resulting in cell division and apoptosis suppression. MiRNA-21 and survivin are both associated with inhibiting the activity of caspase-3 and caspase-7, thus leading to an enhanced therapy effect. The expression level decrease of miRNA-21 and survivin synergistically induced an increase in activity of caspase-3 and caspase-7, leading to better inhibition

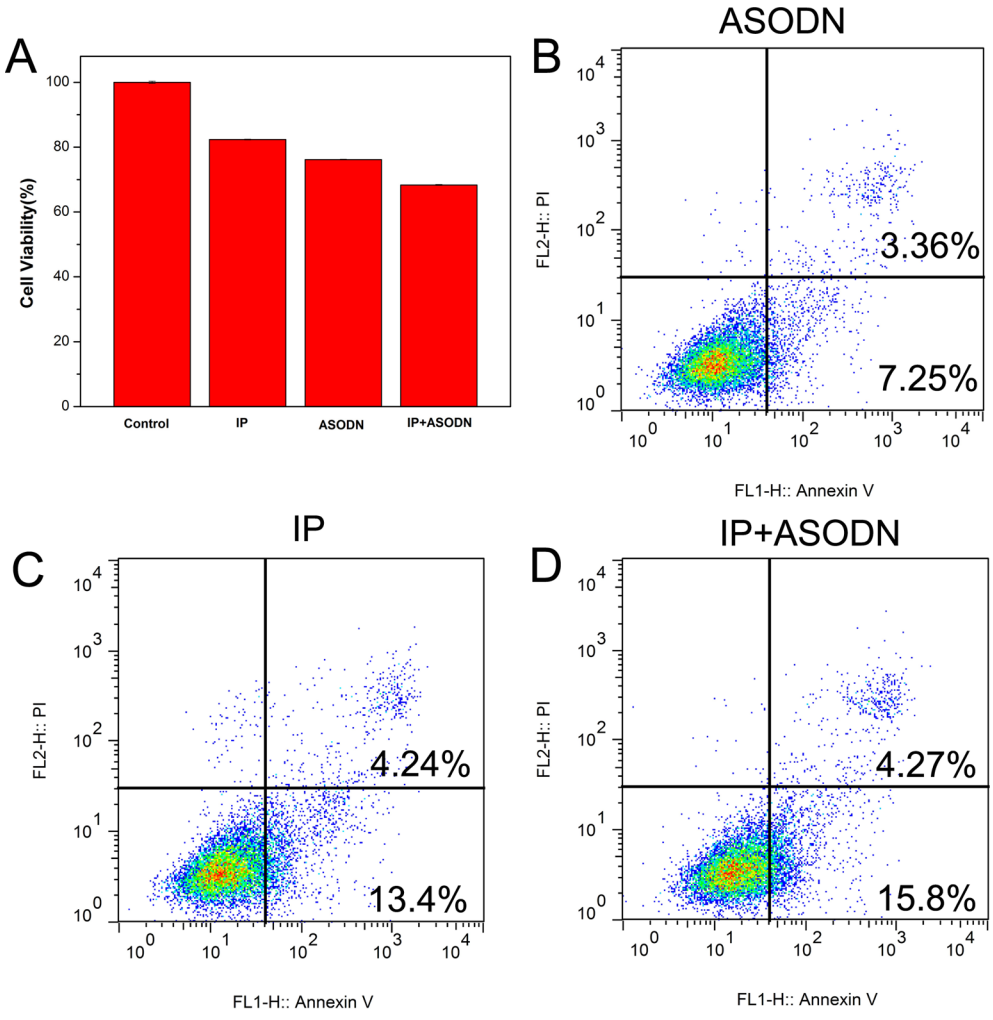

Figure 8. (A) Cell viability of HeLa cells transfected by f-GQDs/ASODN (14 μg/mL, 50 nM loaded ASODN), f-GQDs/IP (14 μg/mL, 50 nM loaded ASODN), and f-GQDs/IP/ASODN (14 μg/mL, 50 nM loaded ASODN and 50 nM IP). Flow cytometric apoptotic analysis of HeLa cell transfected by (B) f-GQDs/ASODN, (C) f-GQDs/IP, and (D) f-GQDs/IP/ASODN at the concentration (14 μg/mL, 50 nM loaded cargos).

DOI: 10.1021/acsami.5b02803
ACS Appl. Mater. Interfaces 2015, 7, 11015−11023

of growth and more apoptosis of the cancer cell. The detailed mechanism of the combined effect requires further exploration in our group for a rational design nanodelivery system in order to improve the gene therapeutic efficacy.

CONCLUSIONS

This work designed a simple and multifunctional fluorescent nanocomposite of GQDs grafted with PEG and PLA for cell imaging, intracellular miRNA regulation, and multiple gene probe delivery in order to enhance gene therapeutic efficacy. The proposed f-GQDs were comprehensively characterized by microscopic and spectroscopic methods including TEM, AFM, XPS, FT-IR, EIS, and UV−vis. Functionalization of GQDs with PEG and PLA significantly improved the optical properties and rendered the f-GQDs with good biocompatibility, low cytotoxicity, and excellent physiological stability. It was discovered that the f-GQDs nanocomposite was an efficient gene nanovector for intracellular miRNAs regulation and imaging analysis. By simultaneously loading gene-targeting agents on f-GQDs, a combined effect for enhancing the therapeutic efficacy was observed. These results may raise possibilities of f-GQDs as a potential platform for simultaneous diagnosis and therapy in the biomedical-related area.

ASSOCIATED CONTENT

Supporting Information

Materials and reagents, materials characterization, AFM of as-prepared GO, TEM images of as-prepared GQDs-PEG, zeta potential of GQDs, GQDs-PEG, and f-GQDs. PL spectra of the GQDs and f-GQDs at different excitation wavelengths and the time-resolved fluorescence spectrum of f-GQDs. The Supporting Information is available free of charge on the ACS Publications website at DOI: 10.1021/acsami.5b02803.

AUTHOR INFORMATION

Corresponding Authors

*Haifeng Dong. Tel.: +86 10 82375840. E-mail: hfdong@ustb.edu.cn.

*Xueji Zhang. Tel./fax: +86 10 82376993. E-mail: zhangxueji@ustb.edu.cn.

*Yue Zhang. E-mail: yuezhang@ustb.edu.cn.

Notes

The authors declare no competing financial interest.

ACKNOWLEDGMENTS

The work was supported by National Natural Science Foundation of China (NSFC Grant No. 21305008), China Postdoctoral Special Foundation (No. 11175039), Ph.D. Programs Foundation of Ministry of Education of China (No.11170197), The Fundamental Research Funds for the Central Universities and the Chinese 1000 Elites program and USTB start-up fund.

REFERENCES

(1) Sinn, P. L.; Sauter, S. L.; Mccray, P. L. Gene Therapy Progress and Prospects: Development of Improved Lentiviral and Retroviral Vectors-Design, Biosafety, and Production. *Gene Ther.* **2005**, *12*, 1089−1098.

(2) Dong, H.; Lei, J.; Ju, H.; Zhi, F.; Wang, H.; Guo, W.; Zhu, Z.; Yan, F. Target-Cell-Specific Delivery, Imaging, and Detection of Intracellular MicroRNA with a Multifunctional SnO_2 Nanoprobe. *Angew. Chem., Int. Ed.* **2012**, *51*, 4607−4612.

(3) Niidome, T.; Huang, L. Gene Therapy Progress and Prospects: Nonviral Vectors. *Gene Ther.* **2002**, *9*, 1647−1652.

(4) Mcnamara, J. O.; Andrechek, E. R.; Wang, Y.; D Viles, K.; Rempel, R. E.; Gilboa, E.; Sullenger, B. A.; Giangrande, P. H. Cell Type-Specific Delivery of SiRNAs with Aptamer-SiRNA Chimeras. *Nat. Biotechnol.* **2006**, *24*, 1005−1015.

(5) Hong, R.; Bai, W.; Zhai, J.; Liu, W.; Li, X.; Zhang, J.; Cui, X.; Zhao, X.; Ye, X.; Deng, Q.; Tiollais, P.; Wen, Y.; Liu, J.; Xie, Y. Novel Recombinant Hepatitis B Virus Vectors Efficiently Deliver Protein and RNA Encoding Genes into Primary Hepatocytes. *J. Virol.* **2013**, *87*, 6615−6624.

(6) Karlsen, T. A.; Brinchmann, J. E. Liposome Delivery of MicroRNA-145 to Mesenchymal Stem Cells Leads to Immunological Off-Target Effects Mediated by RIG-I. *Mol. Ther.* **2013**, *21*, 1169−1181.

(7) Wang, K.; Zhang, X.; Liu, Y.; Liu, C.; Jiang, B.; Jiang, Y. Tumor Penetrability and Anti-Angiogenesis Using IRGD-Mediated Delivery of Doxorubicin-Polymer Conjugates. *Biomaterials* **2014**, *35*, 8735−8747.

(8) Dong, H.; Ding, L.; Yan, F.; Ji, H.; Ju, H. The Use of Polyethylenimine-Grafted Graphene Nanoribbon for Cellular Delivery of Locked Nucleic Acid Modified Molecular Beacon for Recognition of MicroRNA. *Biomaterials* **2011**, *32*, 3875−3882.

(9) Park, K.; Lee, S.; Kang, E.; Kim, K.; Choi, K.; Kwon, I. C. New Generation of Multifunctional Nanoparticles for Cancer Imaging and Therapy. *Adv. Funct. Mater.* **2009**, *19*, 1553−1566.

(10) Bonanni, A.; Chua, C. K.; Zhao, G.; Sofer, Z.; Pumera, M. Inherently Electroactive Graphene Oxide Nanoplatelets as Labels for Single Nucleotide Polymorphism Detection. *ACS Nano* **2012**, *6*, 8546−8551.

(11) Girit, C. O.; Meyer, J. C.; Erni, R.; Rossell, M. D.; Kisielowski, C.; Yang, L.; Park, C. H.; Crommie, M. F.; Cohen, M. L.; Louie, S. G.; Zettl, A. Graphene at the Edge: Stability and Dynamics. *Science* **2009**, *323*, 1705−1708.

(12) Yan, X.; Cui, X.; Li, B.; Li, L. S. Large, Solution-Processable Graphene Quantum Dots as Light Absorbers for Photovoltaics. *Nano Lett.* **2010**, *10*, 1869−1873.

(13) Zhu, S. J.; Zhang, J.; Tang, S.; Qiao, C.; Wang, L.; Wang, H.; Liu, X.; Li, B.; Li, Y.; Yu, W.; Wang, X.; Sun, H.; Yang, B. Surface Chemistry Routes to Modulate the Photoluminescence of Graphene Quantum Dots: from Fluorescence Mechanism to Up-Conversion Bioimaging Applications. *Adv. Funct. Mater.* **2012**, *22*, 4732−4740.

(14) Nurunnabi, M.; Khatun, Z.; Huh, K. M.; Park, S. Y.; Lee, D. Y.; Cho, K. J.; Lee, Y. K. In Vivo Biodistribution and Toxicology of Carboxylated Graphene Quantum Dots. *ACS Nano* **2013**, *7*, 6858−6867.

(15) Zhu, S.; Zhang, J.; Qiao, C.; Tang, S.; Li, Y.; Yuan, W.; Li, B.; Tian, L.; Liu, F.; Hu, R.; Gao, H.; Wei, H.; Zhang, H.; Sun, H.; Yang, B. Strongly Green-Photoluminescent Graphene Quantum Dots for Bioimaging Applications. *Chem. Commun.* **2011**, *47*, 6858−6860.

(16) Lu, C. H.; Yang, H. H.; Zhu, C. L.; Chen, X.; Chen, G. N. A Graphene Platform for Sensing Biomolecules. *Angew. Chem., Int. Ed.* **2009**, *48*, 4785−4787.

(17) He, S.; Song, B.; Li, D.; Zhu, C.; Qi, W.; Wen, Y.; Wang, L.; Song, S.; Fang, H.; Fan, C. A Graphene Nanoprobe for Rapid, Sensitive, and Multicolor Fluorescent DNA Analysis. *Adv. Funct. Mater.* **2010**, *20*, 453−459.

(18) Zheng, X. T.; He, H. L.; Li, C. M. Multifunctional Graphene Quantum Dots-Conjugated Titanate Nanoflowers for Fluorescence-Trackable Targeted Drug Delivery. *RSC Adv.* **2013**, *3*, 24853−24857.

(19) Wang, X. J.; Sun, X.; Lao, J.; He, H.; Cheng, T. T.; Wang, M. Q.; Wang, S. J.; Huang, F. Multifunctional Graphene Quantum Dots for Simultaneous Targeted Cellular Imaging and Drug Delivery. *Colloid. Surf. B, Biointerfaces* **2014**, *122*, 638−644.

(20) Preeti, N.; Shobha, W.; Michelle, L.; Shishanka, W.; Pooja, C.; Dhiman, S. Graphene Quantum Dots Conjugated Albumin Nanoparticles for Targeted Drug Delivery and Imaging of Pancreatic Cancer. *J. Mater. Chem. B* **2014**, *2*, 3190−3195.

DOI: 10.1021/acsami.5b02803
ACS Appl. Mater. Interfaces 2015, 7, 11015−11023

(21) Shen, J.; Zhu, Y.; Yang, X.; Zong, J.; Zhang, J.; Li, C. One-Pot Hydrothermal Synthesis of Graphene Quantum Dots Surface-Passivated by Polyethylene Glycol and Their Photoelectric Conversion under Near-Infrared light. *New J. Chem.* **2012**, *36*, 97−101.
(22) Yang, K.; Feng, L.; Shi, X.; Liu, Z. Nano-Graphene in Biomedicine: Theranostic Applications. *Chem. Soc. Rev.* **2013**, *42*, 530−547.
(23) Dong, H.; Lei, J.; Ding, L.; Wen, Y.; Ju, H.; Zhang, X. MicroRNA: Function, Detection, and Bioanalysis. *Chem. Rev.* **2013**, *113*, 6207−6233.
(24) Chen, C. Z.; Li, L.; Lodish, H. F.; Bartel, D. P. MicroRNAs Modulate Hematopoietic Lineage Differentiation. *Science* **2004**, *303*, 83−86.
(25) Joglekar, M. V.; Joglekar, V. M.; Hardikar, A. A. Expression of Islet-Specific MicroRNAs during Human Pancreatic Development. *Gene Expr. Patterns* **2009**, *9*, 109−113.
(26) Wang, Y.; Keys, D. N.; Au-Young, J. K.; Chen, C. MicroRNAs in Embryonic Stem Cells. *J. Cell. Physiol.* **2009**, *218*, 251−255.
(27) Hatley, M. E.; Patrick, D. M.; Garcia, M. R.; Richardson, J. A.; Bassel-Duby, R.; Van Rooij, E.; Olson, E. N. Modulation of K-Ras-Dependent Lung Tumorigenesis by MicroRNA-21. *Cancer Cell* **2010**, *18*, 282−293.
(28) Ruan, K.; Fang, X.; Ouyang, G. MicroRNAs: Novel Regulators in the Hallmarks of Human Cancer. *Cancer Lett.* **2009**, *285*, 116−126.
(29) Bartel, D. P. MicroRNAs: Genomics, Biogenesis, Mechanism, and Function. *Cell* **2004**, *116*, 281−297.
(30) Gupta, A.; Gartner, J. J.; Sethupathy, P.; Hatzigeorgiou, A. G.; Fraser, N. W. Anti-Apoptotic Function of a MicroRNA Encoded by the HSV-1 Latency-Associated Transcript. *Nature* **2006**, *442*, 82−85.
(31) Guo, Y.; Chen, Z. L.; Zhang, L.; Zhou, F.; Shi, S. S.; Feng, X. L.; Li, B. Z.; Meng, X.; Ma, X.; Luo, M. Y.; Shao, K.; Li, N.; Qiu, B.; Mitchelson, K.; Cheng, J.; He, J. Distinctive MicroRNA Profiles Relating to Patient Survival in Esophageal Squamous Cell Carcinoma. *Cancer Res.* **2008**, *68*, 26−33.
(32) Altieri, D. C. Validating Survivin as a Cancer Therapeutic Target. *Nat. Rev. Cancer* **2003**, *3*, 46−54.
(33) Ryan, B. M.; O'donovan, N.; Duffy, M. J. Survivin: A New Target for Anti-Cancer Therapy. *Cancer Treat. Rev.* **2009**, *35*, 553−562.
(34) Schmitz, M.; Diestelkoetter, P.; Weigle, B.; Schmachtenberg, F.; Stevanovic, S.; Ockert, D.; Rammensee, H. G.; Rieber, E. P. Generation of Survivin-Specific CD8+ T Effector Cells by Dendritic Cells Pulsed with Protein or Selected Peptides. *Cancer Res.* **2000**, *60*, 4845−4849.
(35) Zha, Z.; Zhang, S.; Deng, Z.; Li, Y.; Li, C.; Dai, Z. Enzyme-Responsive Copper Sulphide Nanoparticles for Combined Photoacoustic Imaging, Tumor-Selective Chemotherapy and Photothermal Therapy. *Chem. Commun.* **2013**, *49*, 3455−3457.
(36) Brown, P. K.; Qureshi, A. T.; Moll, A. N.; Hayes, D. J.; Monroe, W. T. Silver Nanoscale Antisense Drug Delivery System for Photoactivated Gene Silencing. *ACS Nano* **2013**, *7*, 2948−2959.
(37) Liu, H.; Chen, D.; Li, L.; Liu, T.; Tan, L.; Wu, X.; Tang, F. Multifunctional Gold Nanoshells on Silica Nanorattles: A Platform for the Combination of Photothermal Therapy and Chemotherapy with Low Systemic Toxicity. *Angew. Chem., Int. Ed.* **2011**, *50*, 891−895.
(38) Zhang, W.; Guo, Z.; Huang, D.; Liu, Z.; Guo, X.; Zhong, H. Synergistic Effect of Chemo-Photothermal Therapy using PEGylated Graphene Oxide. *Biomaterials* **2011**, *32*, 8555−8561.
(39) Yin, Q.; Shen, J. A.; Chen, L. L.; Zhang, Z. W.; Gu, W. W.; Li, Y. P. Overcoming Multidrug Resistance by Co-delivery of Mdr-1 and Survivin-Targeting RNA with Reduction-Responsible Cationic Poly(β-amino esters). *Biomaterials* **2012**, *33*, 6495−6506.
(40) Pisano, F.; Altomare, C.; Cervio, E.; Barile, L.; Rocchetti, M.; Ciuffreda, M. C.; Malpasso, G.; Copes, F.; Mura, M.; Danieli, P.; Viarengo, G.; Zaza, A.; Gnecchi, M. Combination of miRNA499 and miRNA133 Exerts a Synergic Effect on Cardiac Differentiation. *Stem Cells* **2015**, *33*, 1187−1199.
(41) Pan, D.; Zhang, J.; Li, Z.; Wu, M. Hydrothermal Route for Cutting Graphene Sheets into Blue-Luminescent Graphene Quantum Dots. *Adv. Mater.* **2010**, *22*, 734−738.
(42) Eda, G.; Lin, Y. Y.; Mattevi, C.; Yamaguchi, H.; Chen, H. A.; Chen, I. S.; Chen, C. W.; Chhowalla, M. Blue Photoluminescence from Chemically Derived Graphene Oxide. *Adv. Mater.* **2010**, *22*, 505−509.
(43) Gu, W.; Zhang, W.; Li, X.; Zhu, H.; Wei, J.; Li, Z.; Shu, Q.; Wang, C.; Wang, K.; Shen, W.; Kang, F.; Wu, D. Graphene Sheets from Worm-Like Exfoliated Graphite. *J. Mater. Chem.* **2009**, *19*, 3367−3369.
(44) Zhou, X.; Zhang, Y.; Wang, C.; Wu, X.; Yang, Y.; Zheng, B.; Wu, H.; Guo, S.; Zhang, J. Photo-Fenton Reaction of Graphene Oxide: A New Strategy to Prepare Graphene Quantum Dots for DNA Cleavage. *ACS Nano* **2012**, *6*, 6592−6599.
(45) Attal, S.; Thiruvengadathan, R.; Regev, O. Determination of the Concentration of Single-Walled Carbon Nanotubes in Aqueous Dispersions using UV-Visible Absorption Spectroscopy. *Anal. Chem.* **2006**, *78*, 8098−8104.
(46) Li, X.; Wang, X.; Zhang, L.; Lee, S.; Dai, H. Chemically Derived, Ultrasmooth Graphene Nanoribbon Semiconductors. *Science* **2008**, *319*, 1229−1232.
(47) Zheng, L.; Chi, Y.; Dong, Y.; Lin, J.; Wang, B. Electrochemiluminescence of Water-Soluble Carbon Nanocrystals Released Electrochemically from Graphite. *J. Am. Chem. Soc.* **2009**, *131*, 4564−4565.
(48) Sun, X.; Liu, Z.; Welsher, K.; Robinson, J. T.; Goodwin, A.; Zaric, S.; Dai, H. Nano-Graphene Oxide for Cellular Imaging and Drug Delivery. *Nano Res.* **2008**, *1*, 203−212.
(49) Akhavan, O.; Ghaderi, E.; Emamy, H. Nontoxic Concentrations of PEGylated Graphene Nanoribbons for Selective Cancer Cell Imaging and Photothermal Therapy. *J. Mater. Chem.* **2012**, *22*, 20626−20633.
(50) Huang, J.; Zong, C.; Shen, H.; Liu, M.; Chen, B.; Ren, B.; Zhang. Mechanism of Cellular Uptake of Graphene Oxide Studied by Surface-Enhanced Raman Spectroscopy. *Small* **2012**, *8*, 2577−2584.
(51) Shin, S.; Sung, B. J.; Cho, Y. S.; Kim, H. J.; Ha, N. C.; Hwang, J. I.; Chung, C. W.; Jung, Y. K.; Oh, B. H. An Anti-Apoptotic Protein Human Survivin is a Direct Inhibitor of Caspase-3 and-7. *Biochemistry* **2001**, *40*, 1117−1123.
(52) Chan, J. A.; Krichevsky, A. M.; Kosik, K. S. MicroRNA-21 is an Antiapoptotic Factor in Human Glioblastoma Cells. *Cancer Res.* **2005**, *65*, 6029−6033.

DOI: 10.1021/acsami.5b02803
ACS Appl. Mater. Interfaces 2015, 7, 11015−11023